THE JOURNAL OF PHYSICAL CHEMISTRY B

Article

pubs.acs.org/JPCB

A Microscopic View of Phospholipid Insertion into Biological Membranes

Josh V. Vermaas and Emad Tajkhorshid*

Center for Biophysics and Computational Biology, Department Biochemistry, College of Medicine, and Beckman Institute for Advanced Science and Technology, University of Illinois at Urbana−Champaign, Urbana, Illinois 61801, United States

Supporting Information

ABSTRACT: Understanding the process of membrane insertion is an essential step in developing a detailed mechanism, for example, for peripheral membrane protein association and membrane fusion. The highly mobile membrane mimetic (HMMM) has been used to accelerate the membrane association and binding of peripheral membrane proteins in simulations by increasing the lateral diffusion of phospholipid headgroups while retaining an atomistic description of the interface. Through a comparative study, we assess the difference in insertion rate of a free phospholipid into an HMMM as well as into a conventional phospholipid bilayer and develop a detailed mechanistic model of free phospholipid insertion into biological membranes. The mechanistic insertion model shows that successful irreversible association of the free phospholipid to the membrane interface, which results in its insertion, is the rate-limiting step. Association is followed by independent, sequential insertion of the acyl tails of the free phospholipid into the membrane, with splayed acyl tail intermediates. Use of the HMMM is found to replicate the same intermediate insertion states as in the full phospholipid bilayer; however, it accelerates overall insertion by approximately a factor of 3, with the probability of successful association of phospholipid to the membrane being significantly enhanced.

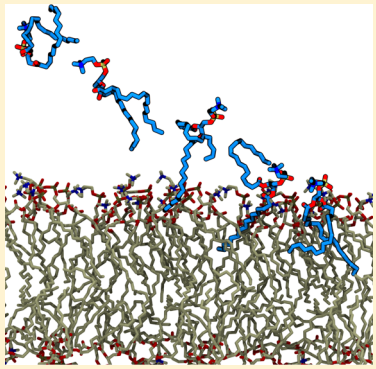

INTRODUCTION

Membrane interfaces play an important role in a wide variety of essential cell functions, including intercellular signaling and energy production.[1−3] Rather than being a passive host, membrane physiocochemical properties such as curvature, stiffness, phospholipid composition, and acyl chain length as well as saturation of the phospholipid tails can modulate membrane-associated processes.[4−7] These physiocochemical properties are determined by phospholipid composition, which is in turn controlled by monomeric phospholipid exchange or vesicular transport.[8] This suggests that the membrane itself is an active participant in orchestrating the symphony of motion across cellular membranes, whether it be by facilitating drug binding,[9−12] mediating the activity of proteins,[13−16] the association and insertion of membrane actors,[17,18] or membrane fusion.[19,20]

In vivo and in vitro experiments are well suited to answer a host of questions related to the membrane interface, such as determining low-energy conformations of membrane-associated proteins,[21] structural details of the membrane itself,[6] and assessing how membrane composition and curvature can impact activity of membrane residents.[15,16,22,23] Single-molecule experiments can also follow the progression of membrane processes at the level of individual molecules laterally across the membrane.[24] However, these methods have their limitations, lacking the temporal resolution required to elucidate mechanistic details of rare and short-lived intermediate states such as spontaneous membrane adsorption and desorption.

Molecular dynamics (MD) simulations can fill these gaps in understanding by bringing to bear the unparalleled spatial and temporal resolutions required to study the process in detail. Simulation studies have been instrumental in unraveling the intricacies of membrane-associated processes such as membrane binding[12,25] and protein conformational changes within the membrane.[26−30]

However, for certain types of processes, such as the membrane insertion of peripheral proteins, the time scales readily accessible to conventional atomistic MD simulations are insufficient to permit the adequate sampling of membrane configuration space needed for insertion. For instance, to simulate the insertion of the GLA domain of blood clotting factor VII, long steered MD simulations were required to capture the anchoring of the protein to the membrane.[31] The root cause of the slow sampling is postulated to be the long acyl tails of conventional membranes tangling with one another,[32] a hypothesis supported by the increase in membrane viscosity with increasing acyl tail length.[33]

The membrane models that evolved responded to these challenges either by extending the time scales accessible by MD simulations through simplifying the system through coarse-grained[34] or implicit membrane models[35−38] or by accelerating the phospholipid dynamics in the same time scale.[39−41] The

Received: October 3, 2013
Revised: December 3, 2013
Published: December 6, 2013

highly mobile membrane mimetic (HMMM) representation accelerates membrane dynamics by simplifying the membrane to its most basic elements, first by reducing the membrane to simply act as a hydrophobic solvent,[32] and then by decorating the solvent with phospholipids where the acyl chains were shortened.[39] These model membranes exhibit a considerably higher lateral phospholipid diffusion constant and greatly accelerate the sampling of the configurational space available to the membrane.[32,39] The current form of the HMMM, with headgroups present but a fluid interior, preserves the essential features of the membrane interface required for the study of insertion processes.

In this report we will use the HMMM representation as well as conventional membrane representations to study a frequently overlooked membrane process, the insertion of free-floating phospholipids into biological membranes. We aim thereby to provide a detailed molecular mechanism for the process and to benchmark the acceleration offered by the HMMM representation for a simple insertion case. Spontaneous phospholipid adsorption/desorption was long ago identified to take place in vitro.[42−45] While frequently overshadowed by vesicular phospholipid traffic, nonvesicular phospholipid trafficking is essential to maintaining the composition of cellular membranes in vivo[8,46] and is the dominant mechanism for phospholipid exchange at low membrane concentrations.[43,47] Furthermore, the mechanism is likely also relevant to lipid recruitment and exchange mediated by proteins.[8]

Despite its importance, to our knowledge no computational studies have focused on the insertion process of a free phospholipid, and as a result there was no detailed mechanism for the adsorption of a free phospholipid into the membrane. Instead, prior computational studies have studied desorption pathways related to membrane fusion, using a coarse reaction coordinate with either the position along the membrane normal of the headgroup[4,48] or the center of mass[20] of the phospholipid as the reaction coordinate to monitor the insertion pathway. Through repeated simulation, we demonstrate a mechanism whereby the geometry of the acyl tails drives the insertion of phospholipids. Comparison between the HMMM and conventional membrane representations reveals that the overall insertion mechanism is independent of membrane representation, and a detailed analysis of structural features shows that essentially the same splayed-tail intermediates to insertion are present in the HMMM and conventional membranes, similar to those found in vesicle fusion studies.[20] While the intermediates are identical, the reaction process is markedly faster in HMMM relative to conventional bilayers, particularly for the association of free phospholipid to the membrane.

COMPUTATIONAL METHODS

A number of replicates of simple membrane systems with varying areas per phospholipid (A_L = 68, 75, 82, 100, and 125 Å^2) were constructed, as reported in Table 1. Each replicate was made by first constructing a 30 × 30 Å membrane patch out of either 1-palmitoyl-2-oleoylphosphatidylcholine (POPC) for conventional membranes or divalerylphosphatidylcholine (DVPC) for HMMM systems. To accomplish this, each phospholipid was placed randomly in the membrane and oriented along the membrane normal (colinear with the z-axis) with a random initial orientation about the long-axis of the phospholipid. The membrane systems are thus either near or above their natural A_L of 68.3 ± 1.5 Å^2,[49] as dictated by the number of phospholipids that were placed. A test insertion phospholipid, in all cases a single POPC molecule, was placed 5 Å above the surface of the membrane, as measured by the minimum distance along the membrane normal between heavy atoms of the test phospholipid and the membrane. The whole system was solvated and ionized to replicate a 100 mM NaCl solution. In HMMM systems, the interior of the membrane was filled with 1,1-dichloroethane (DCLE) through the use of the SOLVATE plugin of Visual Molecular Dynamics (VMD)[50] software to yield a membrane with a thickness of approximately 40 Å,[6,51] matching a conventional POPC bilayer. Examples of fully built systems are shown in Figure 1.

Table 1. Summary of Simulation Systems

lipids per leaflet	approximate A_L (Å^2)	replicate count (full)	replicate count (HMMM)
13	68	48	48
12	75	114	114
11	80	56	56
9	100	56	56
7	125	56	56

Upon construction, each replicate was simulated using NAMD 2.8[52] and the CHARMM36 phospholipid force field[53] until the test insertion phospholipid was judged to be fully inserted into the membrane. While each simulation was only run to insertion, and thus had variable length, the aggregate dynamics time for all the replicates is ∼6 μs. Force integration was performed with 2 fs timesteps, and the forces were calculated with a 12 Å cutoff using a 10 Å switching distance for nonbonded forces. Full-system electrostatic forces were calculated at every other step, using the particle mesh Ewald (PME) method.[54,55] Temperature was maintained at 310 K through Langevin dynamics, using γ = 1 ps^{-1}, and pressure was kept at 1 atm, using a Nosé−Hoover piston[56,57] with period and decay of 200 fs. The system was maintained at fixed area to maintain the initial A_L throughout the simulation.

Analysis Framework. Because of the large number of replicates, automated insertion tests using VMD[50] Tool Command Language (TCL) scripts were devised to determine the time at which a particular insertion event was considered to have taken place and to subdivide the trajectories into their constitutive states. The test phospholipid is said to be *free* in solution when all of its heavy atoms are further than 4 Å away from membrane heavy atoms (e.g., the initial configuration). The test phospholipid is said to be *membrane associated* when any heavy atom is within 4 Å of a membrane heavy atom but neither acyl tail is inserted. A test phospholipid tail is said to be *inserted* when at least one acyl carbon is nearer to the membrane center than 80% of the C5 carbons of the leaflet into which the phospholipid tail is inserting. An equivalent definition for insertion is to say that the z-position of any acyl carbon is within the 40th to 60th percentile of all membrane C5s. From this definition, we view a test phospholipid to be *singly inserted* when one acyl tail is inserted and *doubly inserted* when both acyl tails are inserted. A test phospholipid tail is said to be *fully inserted* when it is both doubly inserted and the z-position of its phosphorus atom is between the 10th and 90th percentile of all membrane phosphates. The times when changes of state took place were noted. While the trajectories were calculated with 2 fs timesteps, the time resolution of these measurements is 10

dx.doi.org/10.1021/jp409854w | J. Phys. Chem. B 2014, 118, 1754−1764

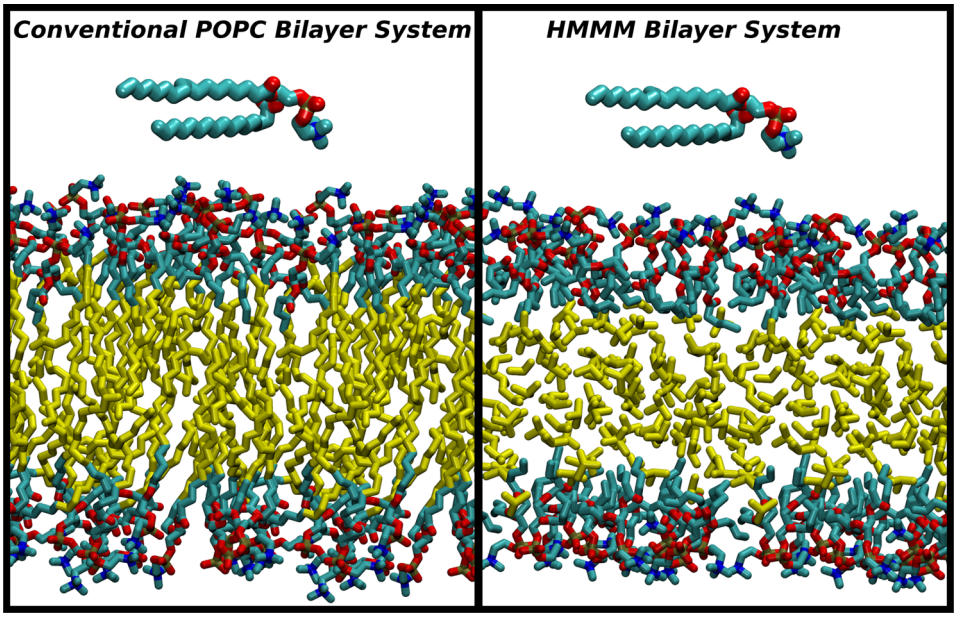

Figure 1. Initial configuration of the simulation systems used to investigate phospholipid insertion into conventional (left) and HMMM (right) membranes. The free-floating phospholipid above the membrane is the test phospholipid, whose insertion into the membrane patch will be monitored. The colors indicate atoms as follows: red, O; blue, N; brown, P; cyan, C. For the conventional bilayer, yellow highlights C atoms replaced by solvent in the corresponding HMMM representation, where the yellow atoms are the carbons and chlorines that make up the organic solvent. All hydrogen atoms, as well as ions and water, have been omitted for clarity.

ps, corresponding to the time evolution between frames in the analysis.

When thinking about the insertion of phospholipids or phospholipid anchors into membranes, oftentimes it suffices to view the process of phospholipid insertion in terms of a single reaction:[42,43]

$$\text{free lipid} \underset{k_r}{\overset{k_f}{\rightleftarrows}} \text{membrane lipid} \tag{1}$$

In the context of physiological membranes, additional inserting phospholipids are easily accommodated into the membrane by a small area expansion. Under these conditions, the insertion rate of a free phospholipid to the bilayer greatly exceeds the rate of desorption, and thus $k_f \gg k_r$. In this regime, the reaction is governed by a first-order rate equation. When applied to an ensemble of single, initially free phospholipids, the result is a simple exponential-decay relationship between the fraction of free phospholipids (χ) and time:

$$\chi(t) = \exp(-k_f t) \tag{2}$$

Viewed another way, we are looking for the first-passage time of the phospholipid insertion into the membrane, which can be considered to be an exponential random variable.[58] However, this broad view, by construction, hides mechanistic details about the process. For instance, consider our proposed alternate version of eq 1, presented schematically in Figure 2, where the complete reaction is subdivided into a set of substitutive molecular events, for example, the sequential insertion of individual phospholipid tails (see eq 3).

$$\begin{gathered}\text{free lipid} \overset{k_1}{\rightleftarrows} \text{membrane associated} \\ \text{membrane associated} \overset{k_2}{\rightleftarrows} \text{singly inserted} \\ \text{singly inserted} \overset{k_3}{\rightleftarrows} \text{doubly inserted} \\ \text{doubly inserted} \overset{k_4}{\rightleftarrows} \text{fully inserted}\end{gathered} \tag{3}$$

The overall process is still intact, which becomes clear as eq 2 is further expanded:

$$\chi(t) = \exp(-k_f t) = \exp\left(-t\left(\sum_{i=1}^{4} k_i^{-1}\right)^{-1}\right) \tag{4}$$

Breaking down the overall reaction into individual steps has additional value, in that it forms a mechanism that can be used to evaluate which steps within the larger process are rate-limiting and how fast a particular step in the reaction is relative to the others. While breaking up the insertion process in this manner is beneficial conceptually, only through the use of MD simulations is it possible to capture the intermediate states and evaluate the rates of transition for each individual step.

In effect, what we propose is to model the insertion process as a Markov chain. Using MD trajectories to build up a Markov model has been done previously.[59−62] Those experiments focused on the dynamics of protein folding, using Markovian analyses to determine the rates of transition along a folding pathway and thus determine the predominant folding pathway.[60,61] In these studies, the disambiguation and assignment of a point in the trajectory to the individual states is the principal problem, and automated procedures are used to separate states.[62]

Modeling phospholipid insertion as a Markov process presents its own unique challenges. Unlike protein folding, where unfolding and refolding happens on an MD time scale,

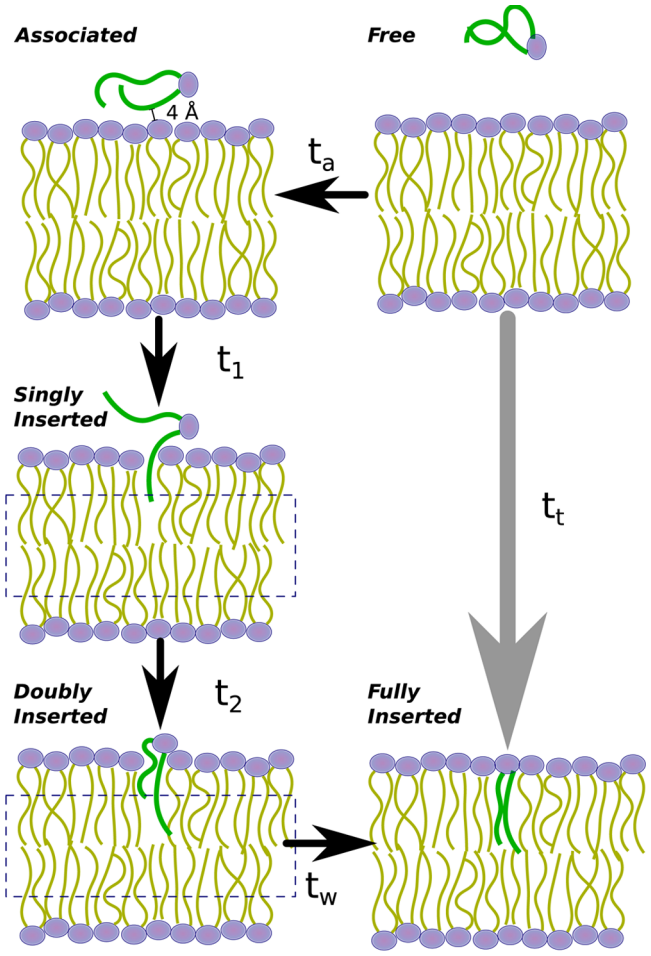

Figure 2. Schematic of the model for phospholipid insertion. The time needed for the overall insertion process of free phospholipid to transition to a fully inserted phospholipid is given as the total time t_t. The intermediate states and their associated times are schematically shown as well. The step between the free and associated phospholipid is termed the association step and is characterized by time t_a. After t_a, at least one heavy atom of the test phospholipid is always within 4 Å of a membrane heavy atom. The tail insertion transition times are given by t_1 and t_2 and indicate the time taken to progress from the associated to the singly inserted states and from the singly inserted to the doubly inserted states, respectively. The wait time for the headgroup reorientation between the doubly inserted and fully inserted states is given by t_w. With these definitions, we have $t_t = t_a + t_1 + t_2 + t_w$. The dashed blue box present in the singly and doubly inserted states represents the threshold level for insertion.

phospholipid insertion is an effectively irreversible process (the free energy cost to remove a phospholipid from a bilayer has been calculated to be between 73 and 80 kJ/mol[4,48]), and as such the number of observed insertions corresponds to the number of simulations. Defining the states between which transitions occur is also key to generating a Markov model. While the states presented in Scheme 3 are conceptually clear, for demarcating phospholipids as being free, associated, or singly or doubly inserted, there are no widely accepted definitions for what these terms mean on a molecular level. Our choice in definitions for the states was designed to provide a molecular mechanism, to allow a fair comparison of HMMM and conventional bilayers by using features present in each representation, and additionally to ensure that the states are truly distinct.

RESULTS

The Overall Picture. The first task is to assess how well the overall process can be described by the basic two-state model presented in eq 1 and if there are substantial differences between the HMMM and conventional membranes at this level of detail. To do this, we examine how the distribution of insertion times fits with the theoretical model given in eq 2. Conventionally an exponential fit is derived by binning the insertion time for each simulation together and then fitting eq 2 to the resulting histogram. The downside to this approach is that the resulting fits are dependent on the chosen histogram bin width.[63] Rather than histogramming the insertion times, we use each gathered insertion time to generate an empirical cumulative distribution function (CDF), which relates the fraction of phospholipids that have inserted to a function of time. The empirical CDF allows us to leverage the statistics we have in a productive manner, weighing each simulation equally to generate an exponential fit. Using the fraction of inserted phospholipids, we fit our empirical results to a CDF of the following form:

$$\text{fraction inserted} = \text{CDF}(t) = 1 - \exp(-k_t t) \quad (5)$$

where k_t corresponds to the rate of the overall reaction ($k_t = k_f$) from eq 1. As shown in Figure 3, the overall insertion behavior

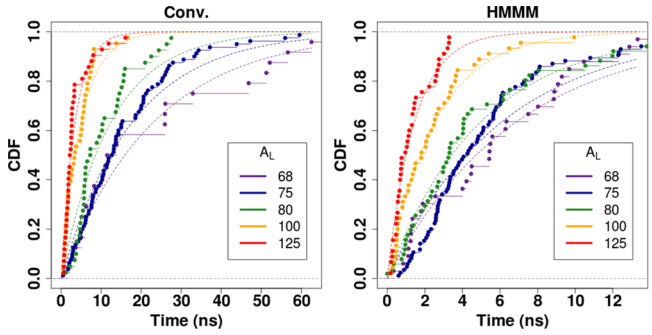

Figure 3. Distribution of total insertion time t_t. The empirical cumulative distribution function (CDF) for the total insertion time of both the conventional (left) and HMMM (right) membranes across a number of phospholipid densities are plotted (●) and fitted to an exponential of the form given in eq 5 (dashed lines). The A_L are distinguished by colors, ranging from 68 Å^2 (violet) to 125 Å^2 (red).

for a particular A_L closely resembles the predictions of the exponential model: an exponential decay of the fraction of phospholipids that remains uninserted as a function of the time needed for full insertion t_t. The reaction rate for the total transition from free phospholipid to fully inserted phospholipid k_t is shown to be linearly dependent on A_L (Figure 4A), suggesting that the increased freedom for individual phospholipids in the membrane accelerates insertion by increasing the number of transient defects in the bilayer that can accommodate the inserting phospholipid. While the trend of increased insertion rate with A_L is consistent across both membrane representations, the rates themselves are representation-dependent. When using near-natural values of A_L (between 68 and 75 Å^2), the overall insertion rate is accelerated in the HMMM representation by a factor between 2.5 and 3.2 with respect to a conventional membrane representation (Figure 4A). Clearly, the higher lateral phospholipid diffusion of the HMMM representation has a significant consistent effect on accelerating the overall phospholipid insertion process.

dx.doi.org/10.1021/jp409854w | J. Phys. Chem. B 2014, 118, 1754−1764

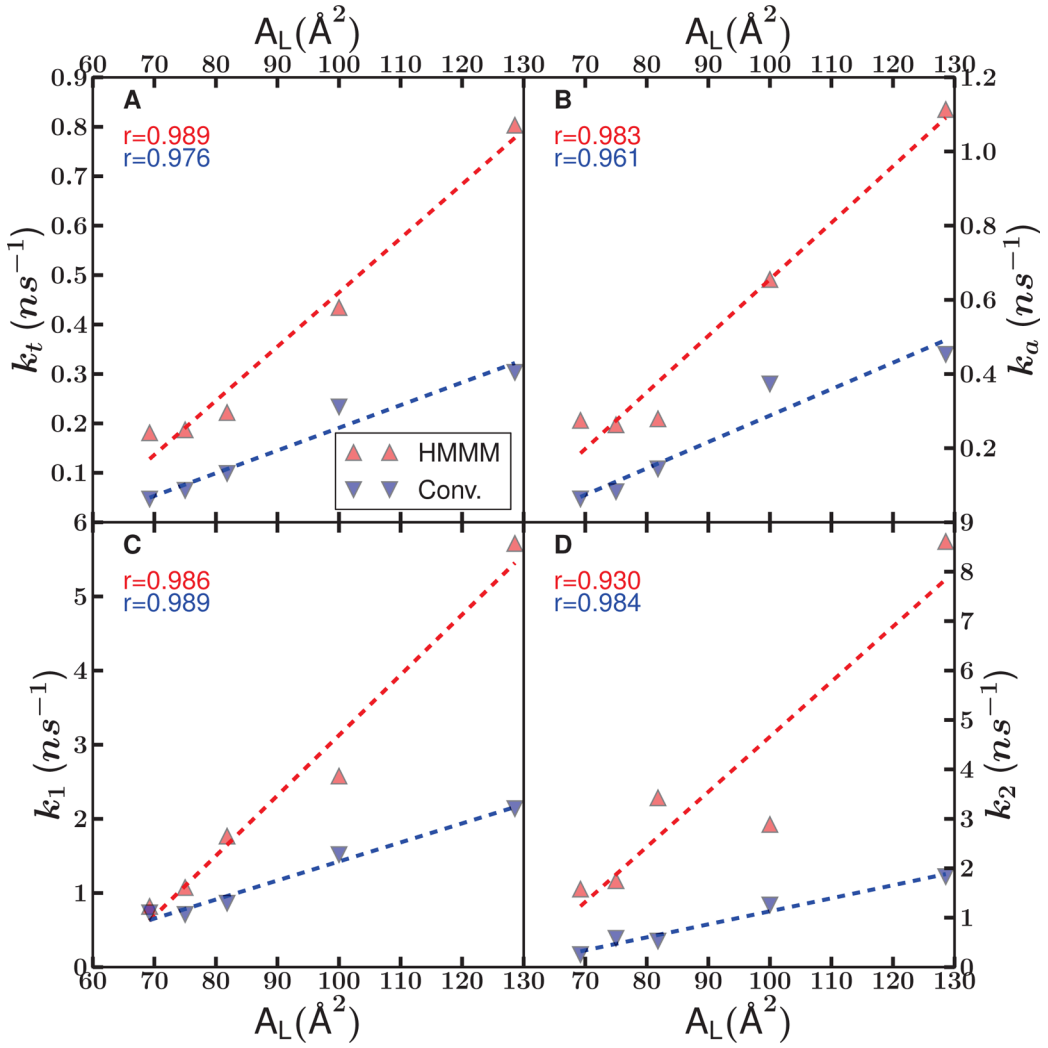

Figure 4. Reaction rates vs A_L. (A) k_t. (B) k_a. (C) k_1. (D) k_2. Plotted symbols (▲ and ▼) represent the reaction rate for a particular membrane insertion step for both HMMM (red) and conventional bilayers (blue). Dotted lines are linear fits to the points, and the *r*-value for each line is reported as well. The rates are extracted from Figure 3 (k_t) and, from the Supporting Information, Figures S1 (k_a), S4 (k_1), and S5 (k_2) via their exponential fits.

Table 2. Rate Table[a]

	HMMM membrane				conventional membrane			
A_L (Å^2)	k_t (ns^{-1})	k_a (ns^{-1})	k_1 (ns^{-1})	k_2 (ns^{-1})	k_t (ns^{-1})	k_a (ns^{-1})	k_1 (ns^{-1})	k_2 (ns^{-1})
68	0.116(3)	0.178(3)	0.71(3)	1.87(5)	0.0315(8)	0.0408(7)	0.62(2)	0.278(5)
75	0.131(3)	0.186(1)	1.03(2)	2.60(6)	0.0484(9)	0.0633(6)	0.64(1)	0.666(9)
80	0.185(5)	0.258(5)	1.34(5)	3.47(6)	0.083(3)	0.151(3)	0.84(3)	0.469(5)
100	0.318(6)	0.49(2)	2.54(5)	3.6(1)	0.158(4)	0.245(9)	1.53(4)	1.33(3)
125	0.52(1)	0.76(3)	4.43(5)	8.0(1)	0.255(9)	0.462(9)	1.83(6)	1.74(5)

[a]The rate constants are the result of fitting each of the empirical cumulative distribution functions to an exponential (Figure 3 (k_t) and, from the Supporting Information, Figures S1 (k_a), S4 (k_1), and S5 (k_2)), with the uncertainty in the last digit reported in parentheses. Note that $k_i^{-1} = k_1^{-1} + k_2^{-1}$.

Splitting Apart the Process: The Two-State Model. The trajectories underlying the measured full-insertion times offer a wealth of information beyond simple end points. We begin by analyzing the insertion process in terms of the granular model in eq 3, determining the rate for each step using the same fitting procedure for an empirical CDF described previously. Following the schematic of Figure 2, the first step for a free phospholipid is to membrane associate. From the distribution of association times t_a (Figure S1 of the Supporting Information), we can measure the rate of membrane association k_a. These rates, along with all other rates calculated, are tabulated in Table 2. The general trend is $k_t \approx k_a$, which suggests that the association step is rate limiting. While we only consider productive membrane associations that immediately precede insertion in our definition of association, unproductive associations are found to be short in duration (Table S1 of the Supporting Information), indicative of nonspecific binding to the membrane before a tail inserts. As the rates for the total

dx.doi.org/10.1021/jp409854w | J. Phys. Chem. B 2014, 118, 1754−1764

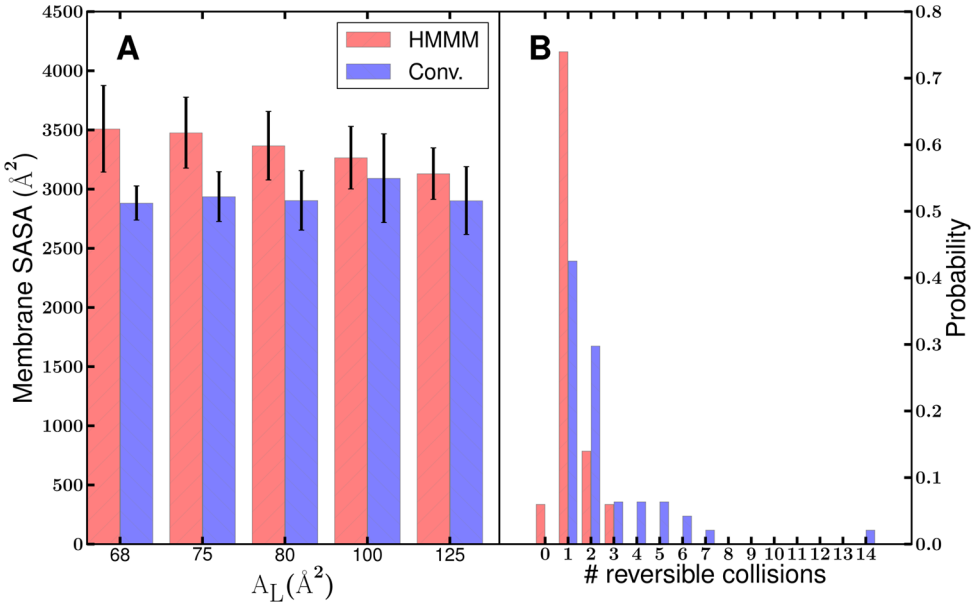

Figure 5. Membrane SASA and reversible collisions. (A) Mean solvent-accessible surface area (SASA) of the membrane measured at the moment the test phospholipid associates to the membrane. The measured SASA takes into account membrane leaflets, such that 1800 Å^2 (30 × 30 × 2) is the minimum possible value, and corresponds to a perfectly flat membrane slab. Thus geometric complexity of the membrane adds ∼1150 Å^2 to the surface area in the case of a conventional membrane and adds as much as ∼1700 Å^2 in an HMMM membrane. This increased interaction surface promotes productive membrane association. (B) Reversible collision distribution compared across membrane representations. A reversible association is defined to be when a test phospholipid heavy atom comes within 4 Å of a membrane heavy atom only to later go beyond 7 Å away again. Conventional membranes have many more of these events, as it is more difficult to find a large enough gap in the membrane to begin inserting the tail into. This histogram only includes data from simulations performed with the lowest A_L, namely, A_L = 68 Å^2 (48 replicates).

insertion process and the association step are similar, the relationship between k_a and A_L is similar to the relationship between k_t and A_L as well, including a significant rate increase for HMMM membranes over conventional bilayers at all A_L (Figure 4B).

The linear dependence of reaction rates on membrane density is an entropic effect, a result of the increased number of transiently forming gaps (defects) in the membrane when the density drops. As a proxy to quantify the number of gaps, we present the membrane solvent-accessible surface area (SASA) in Figure 5A. The SASA values for an HMMM membrane are higher than they are for the corresponding conventional membrane, as the shorter tails of HMMM phospholipids allow for a wider distribution of head groups along the membrane normal. The resulting uneven surface yields an increased surface area available to interact with and promote the insertion of the test phospholipid. As expected, the SASA for conventional bilayers increases with increasing A_L, as the head groups are allowed more freedom to interact with the surrounding aqueous solution rather than with neighboring headgroups. For HMMM bilayers, whose head groups were already mobile, the increase in A_L reduces SASA by flattening the hydrophobic acyl chains along the DCLE membrane core and reducing the mobility of the head groups, leading to a smoother surface with reduced SASA.

Before association, the test phospholipid may collide and interact unproductively with the membrane many times before finding a configuration of phospholipid and membrane suitable for insertion to take place. We quantify this phenomena by counting the number of reversible collisions where the test phospholipid approached the membrane and subsequently left again. The number of reversible collisions (Figure 5B) is highest for conventional membranes, where the slow phospholipids leave only small gaps for the acyl chain to insert into, and thus it takes longer for the test phospholipid to orient itself in a way conducive to insertion. The mean lifetime for such nearly associated states is very short (Table S1 of the Supporting Information), indicating that these collisions are brief encounters where there is little time to wait for a gap in the membrane to appear. These nearly associated states are stabilized by interactions between the headgroups, and last longer with lower A_L. In fact, the phospholipid is usually in a "nearly associated" state sufficiently close to the membrane where significant interactions may take place (Figure S2 of the Supporting Information), but the phospholipid does not find a location to penetrate the membrane before diffusing away momentarily and reorienting. These unproductive collisions are a major contributor to why k_a is reduced in conventional membranes. The more fluid HMMM representation reduces the prevalence of these unproductive interactions and thereby greatly accelerates the slowest step in insertion.

After association, subsequent steps lead to insertion of the acyl tails into the membrane and the repositioning of the headgroup as the phospholipid inserts. While the reaction scheme given in eq 3 splits up the insertion based on the individual tails, we will first look at the combined individual insertion steps. The distributions for the insertion time after association ($t_i = t_t - t_a$) are presented in Figure S3 of the Supporting Information. Insertion is a significantly faster process than association, and as shown in Table 2, the HMMM representation accelerates insertion steps less than it accelerates association. The HMMM representation is preferentially accelerating the rate at which the test phospholipid associates to the membrane, while still faithfully representing details of the system of interest, in this case the actual tail insertion events.

dx.doi.org/10.1021/jp409854w | J. Phys. Chem. B 2014, 118, 1754−1764

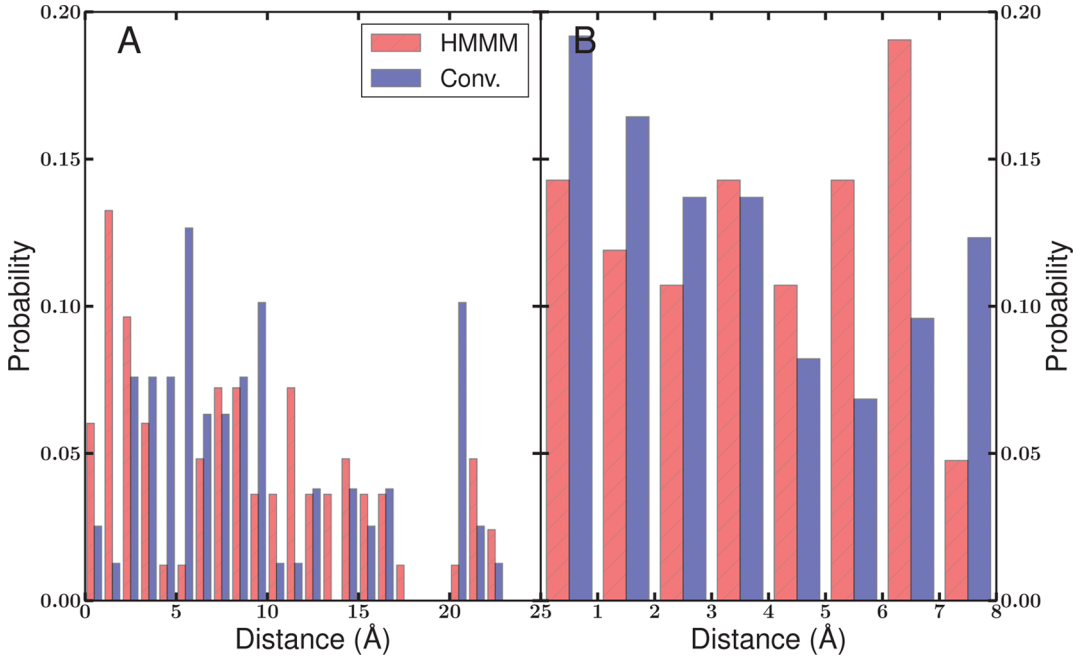

Figure 6. Depth and height distribution at transition points for simulations at A_L = 75 Å^2 (144 replicates). Measured on the left is the minimum height above the insertion threshold of the uninserted tail when the phospholipid transitions to the singly inserted state. The complementary measurement presented on the right is the maximum depth below the insertion threshold of the first inserted tail when the test phospholipid progresses to the doubly inserted state. The distributions are equally wide for both HMMM and full membrane representations. Note that, for visual clarity, the histogram bars for both representations are next to one another and do not touch the bars in adjacent 1 Å bins.

The Details of Insertion: The Four-State Model. Having taken a holistic view of the postassociation insertion process, we now further break apart the insertion step into the three stages given in eq 3. As we monitor the time between association and the time the first phospholipid tail is inserted into the membrane t_1, the first insertion time is exponentially distributed for all A_L (Figure S4 of the Supporting Information) and fits into our model of insertion that describes a succession of exponentially distributed processes. The linear relationship between t_1 and A_L (Figure 4C) suggests that the insertion of the first tail is limited only by the time it takes to find a suitably large gap in the membrane. The rates exhibit a substantial difference between HMMM and conventional membranes at high A_L, while matching at near-natural A_L. At near-natural densities, where gaps are less common, somewhat surprisingly the rate at which the first tail inserts is nearly identical in both HMMM and conventional membranes. As A_L increases, the enhanced mobility of the HMMM phospholipids allows the inserting lipid to push the membrane phospholipids out of the way more readily, leading to the more rapid insertion of one tail than is observed in conventional membranes.

After the insertion of the first tail, one could intuitively expect the insertion of the second tail to follow rapidly thereafter through a cooperativity between the two phospholipid tails. Figure S5 of the Supporting Information shows the distribution of t_2, the time between first and second tail insertions ($t_i = t_1 + t_2$). However, in comparing the rates (Table 2 and Figure 4D), it becomes apparent that the rates for the second tail insertion are not necessarily higher than the rate of first insertion, as we would expect in the case of cooperative insertion. Instead, in conventional membranes, the second tail inserts more slowly than the first. This argues against any cooperativity between the insertion of the first and second tails. Mechanistically this is a result of the second tail not always being associated to the membrane when the first tail inserts. For conventional membranes, waiting for the second tail to insert could be viewed as a second association step. Waiting for the second tail to associate slows down the rate of second tail insertion. However, since the inserted tail tethers the uninserted tail to the membrane, the uninserted tail is in a better position to insert when a membrane gap arises, thus increasing the slope in the relationship between A_L and t_2. The frequent gaps in an HMMM representation are exploited by the uninserted but tethered tail, and thus $k_2 > k_1$ in the HMMM case. There are a few instances where slow test phospholipid dynamics result in the bulges away from the simple exponential fit (Figure S5 of the Supporting Information), where the second tail of the test phospholipid was splayed and needed substantial reorientation after the insertion of the first tail. These bulges make the linearity of the relationship between A_L and t_2 break down for the HMMM case, manifesting in a lower r-value for the linear fit (Figure 4D).

Simply recording timings hides much of the structural information contained within the simulations, especially the geometry of the uninserted tail at transition into the singly inserted state and the location of the previously inserted tail at transition into the doubly inserted state. There are two quantities of interest: how high above the insertion threshold the uninserted tail was when the transition into the singly inserted state occurred, and how far below the insertion threshold the first inserted tail was at the transition into the doubly inserted state. For the A_L with the most sampling, the diversity within these measurements is shown in Figure 6. The wide range of values suggests that the insertions are effectively uncorrelated, and chance alone dictates how far along the "other" tail is at these transitions. This is shown most explicitly in the height above the insertion threshold at the transition to a singly inserted state, where the uninserted tail can be tens of

dx.doi.org/10.1021/jp409854w | J. Phys. Chem. B 2014, 118, 1754−1764

angstroms from the insertion threshold, the free tail floating off in solution rather than interacting with the membrane. These splayed tail intermediates should not be thought of as an unnatural artifact of the simulation conditions; they have also been previously observed in simulations of vesicle fusion and partial desorption.[4,20] The lack of correlation between insertion times is more explicitly shown in Figure 7, where t_1 and t_2 are

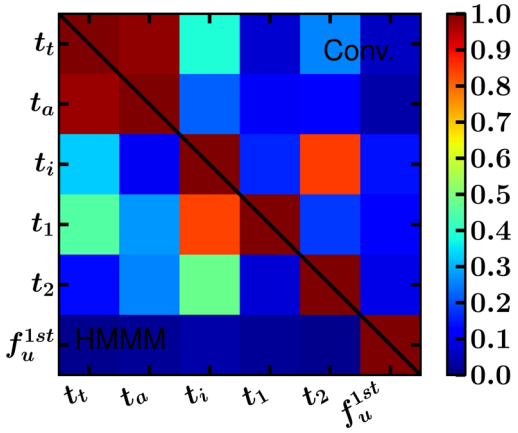

Figure 7. Variance−covariance matrices for six quantities of interest. From the left, these quantities are the total time t_t, the association time t_a, the insertion time $t_i = t_t - t_a = t_1 + t_2 + t_w$, the first tail delay time t_1, the second tail delay time t_2, and if the unsaturated tail inserted first f_u^{first} for the membrane representations at $A_L = 75$ Å^2 (144 replicates). Because of the natural symmetry present in variance−covariance matrices, the halves each represent one membrane type. The lower triangle is for the HMMM representation, and the upper triangle is from a conventional membrane. The variance−covariance matrix at this density is representative for all others. The variance−covariance matrix is a graphical description of what contributes most to the t_t and t_i. For both representations, the t_t is highly correlated with t_a. Weak correlations exist between t_i and its substitutive components, indicating which step took longer. For both membrane representations, the t_1 and t_2 are uncorrelated, suggesting that the two tails insert independently.

shown to be uncorrelated. As there is no evidence to suggest that the phospholipid tails insert in concert, or that there is any correlation at all, the most natural conclusion is that the phospholipid tails insert independently and in a sequential manner, that is, one tail at a time.

Since we propose the phospholipid tails insert independently, it is worth checking the results of an unintentional ancillary experiment that was performed through the choice of test phospholipid. POPC has one unsaturated 18:1 phospholipid tail and a saturated 16:0 tail. While the initial configurations of the test phospholipid should favor the saturated tail inserting first by placing it closer to the membrane (Figure 1), there is no significant bias in favor of the saturated tail. Instead, our simulations reveal only a small, insignificant bias for the saturated tail to insert first (Figure S7 of the Supporting Information), quite likely a consequence of the more extended conformation one expects from saturated phospholipids rather than an initial configuration bias.[64]

Another natural mechanistic detail of interest is regarding the carbon within each tail that inserts first. Intuitively, one might expect the terminal carbon of the acyl chain to nearly always lead insertion. From our simulations, we see a different behavior between the saturated and unsaturated tails of POPC. Figure 8 shows that the intuitive hypothesis is correct for saturated acyl tails, and that terminal carbons are the first to insert. However, for the unsaturated tail, carbons near the point of unsaturation are significantly more likely to insert first than are comparable carbons on the saturated tail. During trajectories where these interior carbons insert first, the tail is bent like a "U" as it enters the bilayer and only later straightens out as the membrane equilibrates. Note that still approximately half of the unsaturated tail insertions show the terminal carbons as the first to insert, making the bent-tail insertion an uncommon occurrence. Since the proportions given in Figure 8 for both the conventional and HMMM representations match, this further suggests that the tail dynamics of the inserting phospholipid are comparable.

Analysis of the final transition, between doubly inserted and fully inserted states, is complicated by the definitions we have devised for these states. As detailed more thoroughly in the Supporting Information, oftentimes t_w is 0, and when it is not, t_w is much shorter than the other transition times. We interpret this to mean that the position of the headgroup is not an independent degree of freedom, but instead simply responds to the insertion state of the acyl tails. Thus it is a fair approximation to say that the transition between doubly inserted and fully inserted states has an infinite rate or equivalently that the doubly inserted and fully inserted states are effectively indistinguishable.

DISCUSSION

The overarching goals here were to delve into the mechanistic details of phospholipid insertion into a membrane and to benchmark the suitability of the HMMM representation for studying membrane insertion in a system where a direct comparison to full membranes is possible. These goals guided our thinking in a number of directions, but it was very clear to us that there had to be sufficient statistics to validate our results. Thus we needed to repeat our simulations to minimize the magnitude of the error caused by limited sampling. The system size was minimized to reduce the cost of individual trajectories for increased repeatability, at the cost of a small membrane. Small membranes have been shown to lead to finite-size effects;[65−67] however, they were not observed in the vast majority of our simulations, and we believe that we have robustly sampled the insertion process for both conventional and HMMM bilayers. The HMMM representation results in the same mechanistically detailed model of membrane insertion when compared to conventional membrane representations with their full acyl tails, with the advantage of a considerable saving in computational effort.

Finding the appropriate reaction coordinate to model insertion was quite a challenge, as the literature is sparse when it comes to postulating a mechanism for naked phospholipid insertion or desorption. Prior studies on the subject have used either the position of the phosphate group[4,48] or the center of mass of the entire phospholipid[20] relative to the membrane normal as their reaction coordinate. However, we observed that these reaction coordinates correlated poorly with what we judged to be insertion progress in our trajectories, as large changes in acyl chain geometry corresponded to small changes in phosphate position. Similarly, by monitoring the center of mass of the test phospholipid, we could not distinguish between a splayed phospholipid with one acyl tail inserted and a phospholipid lying along the membrane interface. This is what drove us to think of how to segment the insertion process into conceptually distinct stages. The

dx.doi.org/10.1021/jp409854w | J. Phys. Chem. B 2014, 118, 1754−1764

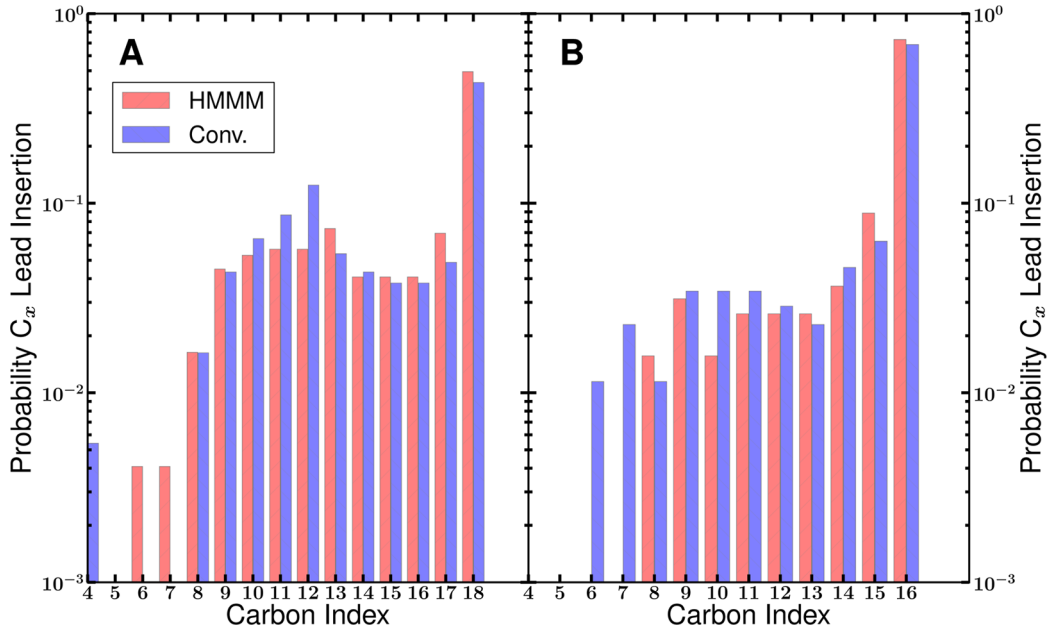

Figure 8. Tail insertion probabilities for (A) unsaturated and (B) saturated acyl tails. For each of the insertions at A_L = 75 Å^2, a record was kept of which carbon was responsible for crossing the insertion threshold first. This yields a distribution for both the saturated and unsaturated tails of the POPC test phospholipid that reveals the geometric dependence of phospholipid tail insertion. The terminal carbons of both tails are typically first to insert, characterized by most of the probability being localized at C18 and C16. However, when the phospholipid is unsaturated, the carbons involved in the natural bend around the unsaturation between C9 and C10 also have an increased probability of being the first carbon to insert.

criteria that emerged are by no means the only possible segmentation of the insertion process, but they do focus on trying to make an equitable comparison between HMMM and conventional bilayers through the available points of reference. This strongly motivated the positioning of the insertion threshold for an acyl tail to be based on membrane C5 atoms, as the HMMM representation has its acyl tails truncated past C5. The atomistic nature of the phospholipid headgroups motivated our contact-based measurement of association, and the reversibility of collisions (Figure 5) suggested that only productive insertions were the relevant quantity. These choices may not be optimal, and are certainly not uniquely determined; however, as a guide to understanding the overall process, we believe that the criteria presented in Analysis Framework are a first step.

Breaking the phospholipid insertion process into the steps given in eq 3 does have broader consequences beyond the simple phospholipid insertion application presented here. If a protein is membrane-anchored through several phospholipid tails, it stands to reason that a similar sequential insertion mechanism would be followed. This also has applications to the energetics of membrane insertion and desorption, as the pathway with the lowest barrier will likely be the path where only one set of hydrophobic contacts is made or broken at a time.[4,20] Finally, exchange of phospholipids between the membrane and specific transport proteins is likely to follow the same mechanism.

Within the details of these results, one can easily lose sight of a key finding, which is that membrane association is rate-limiting, with short (Table S1 of the Supporting Information) and potentially many (Figure 5B) membrane encounters taking place. From the rates presented in Table 2, the initial permanent binding to the membrane is clearly the chief rate-limiting step, an analysis that remains unchanged no matter how "association" is defined. The great surprise is that the insertion of the second tail is a slower process than that of the first in the case of conventional membranes and that there is no apparent cooperativity between the first and second tail insertions. The preferred interpretation is that the insertion of the first tail happens quickly after association, but that the second tail may still need to maneuver into position with respect to the membrane before it inserts. Thus conceptually it may be preferable to break up the second tail insertion into two steps: the association of the second tail to the membrane (with the same entropic cost of associating the first tail), and a similarly accelerated insertion step. That approach was not taken, as there is no guarantee that the insertion of the first tail precedes the membrane association of the second, and would thus introduce additional branches into the reaction scheme in eq 3 beyond the simple Markov chain that was introduced. In principle such a complicated Markov model is within the realms of possibility; however, it would require substantially more simulations to ensure that all possible orderings are sufficiently sampled.

Qualitatively there are only a few differences between the HMMM and conventional membrane representations, which appear to be mainly focused on the kinetics of the association process. The association rate is greatly accelerated by the HMMM through a combination of increasing the surface area available for interaction and increasing the mobility of membrane headgroups. The insertion kinetics, particularly that of the first tail, is not impacted at physiological densities. One can postulate several reasons as to why this occurs, chiefly focusing on the increased mobility brought about by organic solvent. The organic solvent acts as a lubricating layer, promoting the motion of the phosholipids decorating the membrane. This action definitively accelerates the overall insertion process; however, it does so without changing the underlying mechanism. These observations further support the applicability of the HMMM in mechanistic studies, as that

dx.doi.org/10.1021/jp409854w | J. Phys. Chem. B 2014, 118, 1754−1764

representation reduces the computational effort significantly (in the present case by a factor of 4) to obtain the same results.

■ ASSOCIATED CONTENT

Supporting Information

Further discussion of the final step in the schematic mechanism, along with the exponential fits from which the rate constants were determined, are given in the supplement. This material is available free of charge via the Internet at http://pubs.acs.org/.

■ AUTHOR INFORMATION

Corresponding Author

*Email: emad@life.illinois.edu. Tel.: +1 (217) 244-6914. Fax: +1 (217) 244-6078.

Notes

The authors declare no competing financial interest.

■ ACKNOWLEDGMENTS

We gratefully acknowledge the past and present support of both the NIH (R01-GM101048, R01-GM086749, U54-GM087519, and P41-GM104601 to E.T. and Molecular Biophysics Training Grant to J.V.) and the DOE (Computational Sciences Graduate Fellowship to J.V, supported by Grant DE−FG02−97ER25308). Simulations were performed using computer time on XSEDE resources of National Science Foundation (Grant Number MCA06N060) and the Campus Computer cluster Taub at the University of Illinois at Urbana−Champaign.

■ REFERENCES

(1) Liu, L.-N.; Bryan, S. J.; Huang, F.; Yu, J.; Nixon, P. J.; Rich, P. R.; Mullineaux, C. W. Control of Electron Transport Routes Through Redox-Regulated Redistribution of Respiratory Complexes. *Proc. Natl. Acad. Sci. U.S.A.* **2012**, *109*, 11431−11436.

(2) Foyer, C. H.; Neukermans, J.; Queval, G.; Noctor, G.; Harbinson, J. Photosynthetic Control of Electron Transport and the Regulation of Gene Expression. *J. Exp. Bot.* **2012**, *63*, 1637−1661.

(3) Sadiq, S.; Guixa-Gonzalez, R.; Dainese, E.; Pastor, M.; De Fabritiis, G.; Selent, J. Molecular Modeling and Simulation of Membrane Lipid-Mediated Effects on GPCRs. *Curr. Med. Chem.* **2013**, *20*, 22−38.

(4) Grafmüller, A.; Lipowsky, R.; Knecht, V. Effect of Tension and Curvature on the Chemical Potential of Lipids in Lipid Aggregates. *Phys. Chem. Chem. Phys.* **2013**, *15*, 876−881.

(5) Grafmüller, A.; Shillcock, J.; Lipowsky, R. The Fusion of Membranes and Vesicles: Pathway and Energy Barriers from Dissipative Particle Dynamics. *Biophys. J.* **2009**, *96*, 2658−2675.

(6) Nagle, J. F.; Tristram-Nagle, S. Structure of Lipid Bilayers. *Biochim. Biophys. Acta* **2000**, *1469*, 159−195.

(7) Phillips, R.; Ursell, T.; Wiggins, P.; Sens, P. Emerging Roles for Lipids in Shaping Membrane-Protein Function. *Nature* **2009**, *459*, 379−384.

(8) Lev, S. Non-Vesicular Lipid Transport by Lipid-Transfer Proteins and Beyond. *Nat. Rev. Mol. Cell Biol.* **2010**, *11*, 739−750.

(9) Barbacci, D.; Jackson, S. N.; Muller, L.; Egan, T.; Lewis, E. K.; Schultz, J. A.; Woods, A. S. Cellular Membrane Phospholipids Act As a Depository for Quaternary Amine Containing Drugs Thus Competing with the Acetylcholine/Nicotinic Receptor. *J. Proteome Res.* **2012**, *11*, 3382−3389.

(10) Romsicki, Y.; Sharom, F. J. the Membrane Lipid Environment Modulates Drug Interactions with the P-Glycoprotein Multidrug Transporter. *Biochemistry* **1999**, *38*, 6887−6896.

(11) R. Neves, A.; Lucio, M.; L.C. Lima, J.; Reis, S. Resveratrol in Medicinal Chemistry: A Critical Review of Its Pharmacokinetics, Drug-Delivery, and Membrane Interactions. *Curr. Med. Chem.* **2012**, *19*, 1663−1681.

(12) Kopeć, W.; Telenius, J.; Khandelia, H. Molecular Dynamics Simulations of the Interactions of Medicinal Plant Extracts and Drugs with Lipid Bilayer Membranes. *FEBS J.* **2013**, *280*, 2785−2805.

(13) Cerasoli, E.; Ravi, J.; Gregor, C.; Hussain, R.; Siligardi, G.; Martyna, G.; Crain, J.; Ryadnov, M. G. Membrane Mediated Regulation in Free Peptides of HIV-1 Gp41: Minimal Modulation of the Hemifusion Phase. *Phys. Chem. Chem. Phys.* **2012**, *14*, 1277−1285.

(14) Sun, X.; Shi, J.; Delaloye, K.; Yang, X.; Yang, H.; Zhang, G.; Cui, J. the Interface Between Membrane-Spanning and Cytosolic Domains in Ca2+-Dependent K+ Channels Is Involved in β Subunit Modulation of Gating. *J. Neurosci.* **2013**, *33*, 11253−11261.

(15) Ahn, T.; Yun, C.-H.; Kim, H.-R.; Chae, H.-J. Cardiolipin, Phosphatidylserine, and BH4 Domain of Bcl-2 Family Regulate Ca2+/H+ Antiporter Activity of Human Bax Inhibitor-1. *Cell Calcium* **2010**, *47*, 387−396.

(16) Egea-Jiménez, A. L.; Pérez-Lara, A.; Corbalán-Garca, S.; Gómez-Fernández, J. C. Phosphatidylinositol 4,5-Bisphosphate Decreases the Concentration of Ca^{2+}, Phosphatidylserine and Diacylglycerol Required for Protein Kinase C α to Reach Maximum Activity. *PLoS One* **2013**, *8*, e69041.

(17) Vogel, A.; Reuther, G.; Roark, M. B.; Tan, K.-T.; Waldmann, H.; Feller, S. E.; Huster, D. Backbone Conformational Flexibility of the Lipid Modified Membrane Anchor of the Human N-Ras Protein Investigated by Solid-State NMR and Molecular Dynamics Simulation. *Biochim. Biophys. Acta, Biomembr.* **2010**, *1798*, 275−285.

(18) Vogel, A.; Roark, M.; Feller, S. E. A Reinterpretation of Neutron Scattering Experiments on a Lipdated Ras Peptide Using Replica Exchange Molecular Dynamics. *Biochim. Biophys. Acta, Biomembr.* **2012**, *1818*, 219−224.

(19) Markwick, P. R. L.; Pierce, L. C. T.; Goodin, D. B.; McCammon, J. A. Adaptive Accelerated Molecular Dynamics (Ad-AMD) Revealing the Molecular Plasticity of P450cam. *J. Phys. Chem. Lett.* **2011**, *2*, 158−164.

(20) Smirnova, Y. G.; Marrink, S.-J.; Lipowsky, R.; Knecht, V. Solvent-Exposed Tails As Prestalk Transition States for Membrane Fusion at Low Hydration. *J. Am. Chem. Soc.* **2010**, *132*, 6710−6718.

(21) Chill, J. H.; Naider, F. A Solution NMR View of Protein Dynamics in the Biological Membrane. *Curr. Opin. Struct. Biol.* **2011**, *21*, 627−633.

(22) Holzer, R. G.; Park, E.-J.; Li, N.; Tran, H.; Chen, M.; Choi, C.; Solinas, G.; Karin, M. Saturated Fatty Acids Induce C-Src Clustering Within Membrane Subdomains, Leading to JNK Activation. *Cell* **2011**, *147*, 173−184.

(23) Antonny, B. Mechanisms of Membrane Curvature Sensing. *Annu. Rev. Biochem.* **2011**, *80*, 101−123.

(24) Kusumi, A.; Nakada, C.; Ritchie, K.; Murase, K.; Suzuki, K.; Murakoshi, H.; Kasai, R. S.; Kondo, J.; Fujiwara, T. Paradigm Shift of the Plasma Membrane Concept from the Two-Dimensional Continuum Fluid to the Partitioned Fluid: High-Speed Single-Molecule Tracking of Membrane Molecules. *Annu. Rev. Biophys. Biomol. Struct.* **2005**, *34*, 351−378.

(25) Morrissey, J. H.; Tajkhorshid, E.; Rienstra, C. M. Nanoscale Studies of Protein—Membrane Interactions in Blood Clotting. *J. Thromb. Haemostasis* **2011**, *9* (Suppl. 1), 167−167.

(26) Wen, P.-C.; Huang, Z.; Enkavi, G.; Wang, Y.; Gumbart, J.; Tajkhorshid, E. Molecular Mechanisms of Active Transport Across the Cellular Membrane. In *Molecular Simulations and Biomembranes: From Biophysics to Function*; Biggin, P., Sansom, M., Eds.; Royal Society of Chemistry: London, 2010; pp 248−286.

(27) Shaikh, S. A.; Wen, P.-C.; Enkavi, G.; Huang, Z.; Tajkhorshid, E. Capturing Functional Motions of Membrane Channels and Transporters with Molecular Dynamics Simulation. *J. Comput. Theor. Nanosci.* **2010**, *7*, 2481−2500.

(28) Shimamura, T.; Weyand, S.; Beckstein, O.; Rutherford, N. G.; Hadden, J. M.; Sharples, D.; Sansom, M. S. P.; Iwata, S.; Henderson, P. J. F.; Cameron, A. D. Molecular Basis of Alternating Access Membrane

Transport by the Sodium-Hydantoin Transporter Mhp1. *Science* **2010**, *328*, 470−473.
(29) Nury, H.; Poitevin, F.; Van Renterghem, C.; Changeux, J.-P.; Corringer, P.-J.; Delarue, M.; Baaden, M. One-Microsecond Molecular Dynamics Simulation of Channel Gating in a Nicotinic Receptor Homologue. *Proc. Natl. Acad. Sci. U.S.A.* **2010**, *107*, 6275−6280.
(30) Kruse, A. C.; Hu, J.; Pan, A. C.; Arlow, D. H.; Rosenbaum, D. M.; Rosemond, E.; Green, H. F.; Liu, T.; Chae, P. S.; Dror, R. O.; et al. Structure and Dynamics of the M3Muscarinic Acetylcholine Receptor. *Nature* **2012**, *482*, 552−556.
(31) Ohkubo, Y. Z.; Tajkhorshid, E. Distinct Structural and Adhesive Roles of Ca_{2+} in Membrane Binding of Blood Coagulation Factors. *Structure* **2008**, *16*, 72−81.
(32) Arcario, M. J.; Ohkubo, Y. Z.; Tajkhorshid, E. Capturing Spontaneous Partitioning of Peripheral Proteins Using a Biphasic Membrane-Mimetic Model. *J. Phys. Chem. B* **2011**, *115*, 7029−7037.
(33) den Otter, W. K.; Shkulipa, S. A. Intermonolayer Friction and Surface Shear Viscosity of Lipid Bilayer Membranes. *Biophys. J.* **2007**, *93*, 423−433.
(34) Marrink, S. J.; Risselada, H. J.; Yefimov, S.; Tieleman, D. P.; de Vries, A. H. The MARTINI Force Field: Coarse Grained Model for Biomolecular Simulations. *J. Phys. Chem. B* **2007**, *111*, 7812−7824.
(35) Im, W.; Feig, M.; Brooks, C. L., III An Implicit Membrane Generalized Born Theory for the Study of Structure, Stability, and Interactions of Membrane Proteins. *Biophys. J.* **2003**, *85*, 2900−2918.
(36) Panahi, A.; Feig, M. Dynamic Heterogeneous Dielectric Generalized Born (DHDGB): An Implicit Membrane Model with a Dynamically Varying Bilayer Thickness. *J. Chem. Theor. Comput.* **2013**, *9*, 1709−1719.
(37) Lazaridis, T. Effective Energy Function for Proteins in Lipid Membranes. *Proteins* **2003**, *52*, 176−192.
(38) Ulmschneider, M. B.; Sansom, M. S. P.; Di Nola, A. Properties of Integral Membrane Protein Structures: Derivation of an Implicit Membrane Potential. *Proteins* **2005**, *59*, 252−265.
(39) Ohkubo, Y. Z.; Pogorelov, T. V.; Arcario, M. J.; Christensen, G. A.; Tajkhorshid, E. Accelerating Membrane Insertion of Peripheral Proteins with a Novel Membrane Mimetic Model. *Biophys. J.* **2012**, *102*, 2130−2139.
(40) Hamelberg, D.; Mongan, J.; McCammon, J. A. Accelerated Molecular Dynamics: A Promising and Efficient Simulation Method for Biomolecules. *J. Chem. Phys.* **2004**, *120*, 11919−11929.
(41) Pierce, L. C.; Salomon-Ferrer, R.; Augusto, F.; de Oliveira, C.; McCammon, J. A.; Walker, R. C. Routine Access to Millisecond Time Scale Events with Accelerated Molecular Dynamics. *J. Chem. Theory Comput.* **2012**, *8*, 2997−3002.
(42) Martin, F. J.; MacDonald, R. C. Phospholipid Exchange Between Bilayer Membrane Vesicles. *Biochemistry* **1976**, *15*, 321−327.
(43) McLean, L. R.; Phillips, M. C. Mechanism of Cholesterol and Phosphatidylcholine Exchange or Transfer Between Unilamellar Vesicles. *Biochemistry* **1981**, *20*, 2893−2900.
(44) Roseman, M. A.; Thompson, T. E. Mechanism of the Spontaneous Transfer of Phospholipids Between Bilayers. *Biochemistry* **1980**, *19*, 439−444.
(45) Jones, J. D.; Thompson, T. E. Mechanism of Spontaneous, Concentration-Dependent Phospholipid Transfer Between Bilayers. *Biochemistry* **1990**, *29*, 1593−1600.
(46) Lev, S. Nonvesicular Lipid Transfer from the Endoplasmic Reticulum. *Cold Spring Harbor Perspect. Biol.* **2012**, *4*, a013300.
(47) Nichols, J. W.; Pagano, R. E. Kinetics of Soluble Lipid Monomer Diffusion Between Vesicles. *Biochemistry* **1981**, *20*, 2783−2789.
(48) Tieleman, D. P.; Marrink, S.-J. Lipids out of Equilibrium: Energetics of Desorption and Pore Mediated Flip-Flop. *J. Am. Chem. Soc.* **2006**, *128*, 12462−12467.
(49) Kučerka, N.; Tristram-Nagle, S.; Nagle, J. F. Structure of Fully Hydrated Fluid Phase Lipid Bilayers with Monounsaturated Chains. *J. Membr. Biol.* **2005**, *208*, 193−202.
(50) Humphrey, W.; Dalke, A.; Schulten, K. VMD—Visual Molecular Dynamics. *J. Mol. Graphics* **1996**, *14*, 33−38.
(51) Lewis, B. A.; Engelman, D. M. Lipid Bilayer Thickness Varies Linearly with Acyl Chain Length in Fluid Phosphatidylcholine Vesicles. *J. Mol. Biol.* **1983**, *166*, 211−217.
(52) Phillips, J. C.; Braun, R.; Wang, W.; Gumbart, J.; Tajkhorshid, E.; Villa, E.; Chipot, C.; Skeel, R. D.; Kale, L.; Schulten, K. Scalable Molecular Dynamics with NAMD. *J. Comput. Chem.* **2005**, *26*, 1781−1802.
(53) Klauda, J. B.; Venable, R. M.; Freites, J. A.; O'Connor, J. W.; Tobias, D. J.; Mondragon-Ramirez, C.; Vorobyov, I.; MacKerell, A. D., Jr.; Pastor, R. W. Update of the CHARMM All-Atom Additive Force Field for Lipids: Validation on Six Lipid Types. *J. Phys. Chem. B* **2010**, *114*, 7830−7843.
(54) Darden, T.; York, D.; Pedersen, L. G. Particle Mesh Ewald: An $N\cdot\log(N)$ Method for Ewald Sums in Large Systems. *J. Chem. Phys.* **1993**, *98*, 10089−10092.
(55) Essmann, U.; Perera, L.; Berkowitz, M. L.; Darden, T.; Lee, H.; Pedersen, L. G. A Smooth Particle Mesh Ewald Method. *J. Chem. Phys.* **1995**, *103*, 8577−8593.
(56) Martyna, G. J.; Tobias, D. J.; Klein, M. L. Constant Pressure Molecular Dynamics Algorithms. *J. Chem. Phys.* **1994**, *101*, 4177−4189.
(57) Feller, S. E.; Zhang, Y.; Pastor, R. W.; Brooks, B. R. Constant Pressure Molecular Dynamics Simulation: The Langevin Piston Method. *J. Chem. Phys.* **1995**, *103*, 4613−4621.
(58) Nobile, A. G.; Ricciardi, L. M.; Sacerdote, L. Exponential Trends of Ornstein—Uhlenback First-Passage-Time Densities. *J. Appl. Probab.* **1985**, *22*, 360−369.
(59) Swope, W. C.; Pitera, J. W.; Suits, F. Describing Protein Folding Kinetics by Molecular Dynamics Simulations. 1. Theory. *J. Phys. Chem. B* **2004**, *108*, 6571−6581.
(60) Voelz, V. A.; Bowman, G. R.; Beauchamp, K.; Pande, V. S. Molecular Simulation of Ab Initio Protein Folding for a Millisecond Folder NTL9(1−39). *J. Am. Chem. Soc.* **2010**, *132*, 1526−1528.
(61) Elmer, S. P.; Park, S.; Pande, V. S. Foldamer Dynamics Expressed Via Markov State Models. I. Explicit Solvent Molecular-Dynamics Simulations in Acetonitrile, Chloroform, Methanol and Water. *J. Chem. Phys.* **2005**, *123*, 114902.
(62) Chodera, J. D.; Singhal, N.; Pande, V. S.; Dill, K. A.; Swope, W. C. Automatic Discovery of Metastable States for the Construction of Markov Models of Macromolecular Conformational Dynamics. *J. Chem. Phys.* **2007**, *126*, 155101.
(63) Berg, B. A.; Harris, R. C. From Data to Probability Densities Without Histograms. *Comput. Phys. Commun.* **2008**, *179*, 443−448.
(64) Heller, H.; Schaefer, M.; Schulten, K. Molecular Dynamics Simulation of a Bilayer of 200 Lipids in the Gel and in the Liquid Crystal-Phases. *J. Phys. Chem.* **1993**, *97*, 8343−8360.
(65) Lee, S.-J.; Song, Y.; Baker, N. A. Molecular Dynamics Simulations of Asymmetric NaCl and KCl Solutions Separated by Phosphatidylcholine Bilayers: Potential Drops and Structural Changes Induced by Strong Na^+-Lipid Interactions and Finite Size Effects. *Biophys. J.* **2008**, *94*, 3565−3576.
(66) Castro-Román, F.; Benz, R. W.; White, S. H.; Tobias, D. J. Investigation of Finite System-Size Effects in Molecular Dynamics Simulations of Lipid Bilayers. *J. Phys. Chem. B* **2006**, *110*, 24157−24164.
(67) Yeh, I.-C.; Hummer, G. System-Size Dependence of Diffusion Coefficients and Viscosities from Molecular Dynamics Simulations with Periodic Boundary Conditions. *J. Phys. Chem. B* **2004**, *108*, 15873−15879.